

Research Article

Effects of HD-tDCS on Resting-State Functional Connectivity in the Prefrontal Cortex: An fNIRS Study

M. Atif Yaqub,¹ Seong-Woo Woo,¹ and Keum-Shik Hong^{1,2} 

¹School of Mechanical Engineering, Pusan National University, Busan 46241, Republic of Korea

²Department of Cogno-Mechatronics Engineering, Pusan National University, Busan 46241, Republic of Korea

Correspondence should be addressed to Keum-Shik Hong; kshong@pusan.ac.kr

Received 4 June 2018; Revised 31 August 2018; Accepted 17 September 2018; Published 1 November 2018

Academic Editor: Vincent Labatut

Copyright © 2018 M. Atif Yaqub et al. This is an open access article distributed under the Creative Commons Attribution License, which permits unrestricted use, distribution, and reproduction in any medium, provided the original work is properly cited.

Functional connectivity is linked to several degenerative brain diseases prevalent in our aging society. Electrical stimulation is used for the clinical treatment and rehabilitation of patients with many cognitive disorders. In this study, the effects of high-definition transcranial direct current stimulation (HD-tDCS) on resting-state brain networks in the human prefrontal cortex were investigated by using functional near-infrared spectroscopy (fNIRS). The intrahemispheric as well as interhemispheric connectivity changes induced by 1 mA HD-tDCS were examined in 15 healthy subjects. Pearson correlation coefficient-based correlation matrices were generated from filtered time series oxyhemoglobin (ΔHbO) signals and converted into binary matrices. Common graph theory metrics were computed to evaluate the network changes. Systematic interhemispheric, intrahemispheric, and intraregional connectivity analyses demonstrated that the stimulation positively affected the resting-state connectivity in the prefrontal cortex. The poststimulation connectivity was increased throughout the prefrontal region, while focal HD-tDCS effects induced an increased rate of connectivity in the stimulated hemisphere. The graph theory metrics clearly distinguished the prestimulation and poststimulation networks for a range of thresholds. The results of this study suggest that HD-tDCS can be used to increase functional connectivity in the prefrontal cortex. The increase in functional connectivity can be explored clinically for neurorehabilitation of patients with degenerative brain diseases.

1. Introduction

Today's rapidly aging society is increasingly confronting degenerative brain diseases, such as mild cognitive impairment (MCI) and Alzheimer's disease (AD). Patients with AD face difficulties in their daily tasks due to impairments in cognitive functions like working memory, episodic memory, and executive attention [1, 2]. AD is considered a disconnection syndrome in which the connectivity between different areas of the brain is disturbed; however, efficient connectivity is vital for optimal performance of our day-to-day tasks [3]. The ability to hold and manipulate items in our conscious awareness is called working memory [4]. Due to the central role of working memory in cognition, researchers have investigated potential methods to expand its capacity [5]. The prefrontal cortex is involved in working memory and several executive tasks [6]. Recently, functional near-infrared spectroscopy (fNIRS) has been employed to

study the functional activation and connectivity in relation to working memory, AD, and multiple neuropsychiatric disorders [7] such as schizophrenia [8], various types of affective disorders [9–14], and the treatment and rehabilitative effects in psychiatric disorders [15]. Functional connectivity in the human brain is critical for the performance of our daily tasks. Therefore, this study was conducted to develop a better understanding of resting-state functional connectivity and its dynamic changes in light of stimulation.

Transcranial direct current stimulation (tDCS) is a technique used to deliver small amounts of electric current to modulate the excitability of neural populations in different regions of the brain [16]. This noninvasive stimulation technique has been increasingly applied to various brain regions of healthy as well as diseased subjects [17], because it is well tolerated, safe, and inexpensive compared to other techniques involving invasive stimulation [18–21] which is based on nerve signal information [22]. Several studies have used

tDCS to investigate the polarity-specific effects that are not limited to the stimulated site [23–27]. These findings suggest that tDCS induces functional connectivity changes in the brain. Most research groups have used patch electrodes (5 cm × 7 cm saline-soaked sponge electrode pairs) to study the effects of prefrontal cortical stimulation on working memory [4], functional connectivity [28, 29], hemodynamic responses [30, 31], and brain perfusion [32]. Due to the limitations of directly measuring electric fields in tDCS, researchers have modeled the currents between electrodes to predict the passage of tDCS current through brain regions. These modeling studies have been applied to determine the most favorable electrode configuration [33] and multiple small-electrode (~3 cm²) high-definition (HD) montages to control the distribution of the current applied to a specific brain region [34]. In a study using anodal HD-tDCS, one anode electrode was placed at the center and four return electrodes were placed approximately 3.5 cm away from the anode in a ring configuration [35]. HD-tDCS has been used to investigate a method to control the electric field and thereby precisely stimulate a target cortical region [36, 37] to potentially increase the long-term excitability aftereffects [38].

Neuronal activity is directly related to cerebral blood flow [39]. A variety of neuroimaging techniques that measure cerebral hemodynamic changes have been used to study neuronal activities in the human brain [40]. Of these techniques, functional magnetic resonance imaging (fMRI) and positron emission tomography (PET) are widely used to measure blood oxygen level-dependent signals and glucose metabolism, respectively, which reflect neuronal activity in the brain. Because fMRI and PET are immobile, bulky, costly, and have low temporal resolution, these techniques are not suitable for continuous and routine monitoring. In addition, fMRI measurements restrict their use with tDCS because of the current flow in the brain, which produces artifacts and/or distorted fMRI images. tDCS generates a magnetic field that interferes with MRI imaging, which is based on controlled magnetic field distributions [41]. In addition, the use of PET is limited due to concerns regarding its invasiveness and radiation from the injected radiolabels [42]. The portable and noninvasive nature of electroencephalography (EEG) makes it suitable for detecting neurophysiological changes [43] during HD-tDCS [44]. However, the use of EEG is limited by biophysical limits in volume conduction imposed by the scalp, skull, and brain, which limits its spatial resolution, and by the need to remove artifacts induced by the tDCS-induced currents.

Some limitations of the aforementioned imaging technologies can be overcome by fNIRS. fNIRS is a portable, noninvasive, and repeatable method that measures the oxygenation state of hemoglobin in the multilayer tissues [45, 46]. The infrared light-absorbing property of this technique uses the near-infrared light in the 650–1000 nm range to measure blood oxyhemoglobin (HbO) and deoxyhemoglobin (HbR) [47, 48]. The near-infrared light is emitted through the scalp into the brain, and the photons that pass through the brain tissues are measured by detectors placed on the scalp at specified locations. Because fNIRS uses optic-based measurements of light intensity, electrically induced artifacts do not affect it, which makes its use desirable for studying the effects

of tDCS [49, 50]. Therefore, fNIRS has many advantages over other neuroimaging modalities; its application has great potential in studying the functional imaging of the brain [51], perception and cognition [52], behavioral and cognitive neurodevelopment [53, 54], somatosensory and bundled optode configuration [55, 56], stroke and brain injury [57, 58], and brain-computer interfaces [59, 60]. Moreover, various studies have used fNIRS to investigate functional connectivity in different brain regions [61–65].

The purpose of this study was to investigate the relationship of the application of HD-tDCS to examine the functional connectivity in the prefrontal cortex of both hemispheres with the use of fNIRS to simultaneously measure hemodynamic changes. We hypothesized that the application of HD-tDCS would improve/increase the level of hemodynamic response and the resulting functional connectivity under the stimulated area. For the HD-tDCS, one anode and four return electrodes were attached to the prefrontal cortex in addition to the fNIRS probes. This setup allowed us to investigate two issues: (i) the effects of the application of HD-tDCS on hemodynamic responses in the prefrontal region and (ii) the effects of HD-tDCS on functional connectivity. To the best of our knowledge, this is the first fNIRS study to explore the effects of HD-tDCS on brain functional connectivity.

2. Materials and Methods

2.1. Subjects. To evaluate the effects of HD-tDCS using fNIRS, 15 male subjects (mean ± standard deviation, age: 28.5 ± 2.5 years) participated in the experiment. Since the research scope/objective was not gender-related, only male subjects were recruited/volunteered for the experiment due to the uniformity of head size and shorter hair. All subjects were healthy. None had a history of any neurological or psychiatric disorders or head injuries, and no one used neuroleptic, hypnotic, or antiseizure medications. All participants gave written consent after they received a description of the study procedures and associated risks prior to the experiment. The study conformed to the recommendations of the local Human Research Ethics Committee, which are in accordance with the latest Declaration of Helsinki [66].

2.2. Experimental Paradigm. As shown in Figure 1, the experimental paradigm of the study consists of three stages: prestimulation, stimulation, and poststimulation. The experiment lasted for 25 minutes, which consisted of a 5 min prestimulation phase, a 10 min stimulation phase, and, finally, a 10 min poststimulation phase. The subjects were asked to lie comfortably on a clinical bed in Fowler's position and to keep their eyes open in order to avoid falling asleep during the experiment. The positions of the HD-tDCS electrodes were first marked on the subject's forehead according to the specially designed guide, and the electrodes were then placed at the designated marks. The fNIRS probes for recording and HD-tDCS electrodes for stimulation were simultaneously held in the designated places of a specially designed polyurethane foam headgear. During the first phase, the fNIRS data were collected to acquire the baseline signal. In

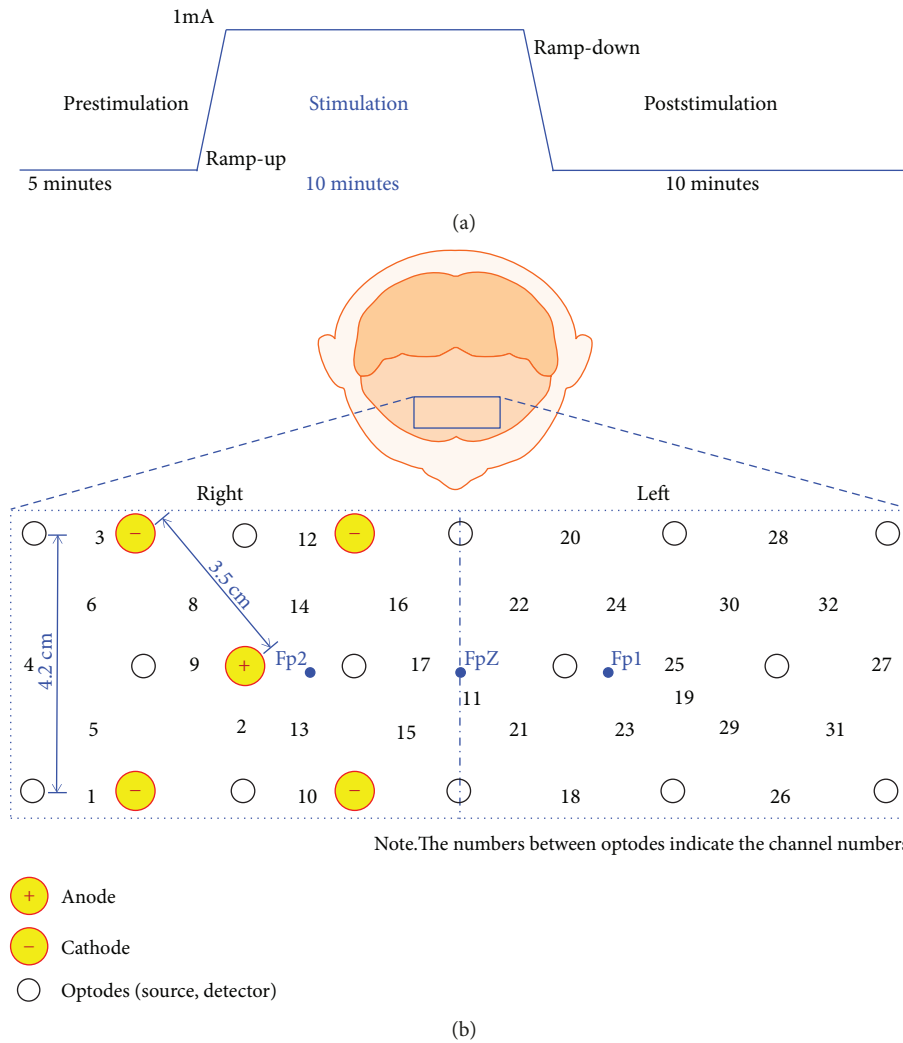


FIGURE 1: (a) Experimental paradigm and (b) simultaneous arrangement of fNIRS optodes and HD-tDCS electrodes.

the second phase, in addition to the continuous fNIRS recordings, active stimulation was applied, ramped up to 1 mA within 15 s, and then maintained at this level during the entire phase, followed by a ramp-down for the last 15 s. In the final phase of the experiment, fNIRS data were acquired to visualize the aftereffects of the stimulation.

2.3. HD-tDCS. Stimulation was delivered by a battery-driven Starstim tCS system (Neuroelectronics, Barcelona, Spain). The system has a total capacity of eight electrodes, with five electrodes used in an anodal 4×1 HD-tDCS electrode configuration. Each electrode is made of AgCl, and each has a diameter of 1 cm. The central anodal electrode and four return electrodes (cathodes) were attached to the skin with conduction-enhancing gel-filled foam (Kendall™ Conductive Adhesive Hydrogel; Medtronic, Minneapolis, MN, USA). The electrodes were used only once per subject and were changed such that a new electrode was used in each experiment. The HD-tDCS electrodes (yellow larger circles in Figure 1) were positioned on the right side of the prefrontal cortex over the eyebrow with 3.5 cm separating the anode from all returning electrodes. The current capacity of the

stimulation through the anode was set to 1 mA, and each return electrode was configured to receive an equal amount of current at 25% of the anodal current. The device communicates via Bluetooth with its own software (Neuroelectronics® Instrument Controller 2.0; Neuroelectronics) running on a laptop computer. The stimulation protocol was programmed to include the electrode selection/placement (in this study, one anode and four return electrodes) and the current distribution setting (in this study, 25% per return electrode) in the software.

2.4. fNIRS Data Acquisition. The fNIRS data were acquired using a continuous-wave fNIRS imaging device (dynamic near-infrared optical tomography (DYNOT); NIRx Medical Technologies, USA). The system was used to continuously measure the changes of the HbO and HbR concentrations in 32 channels covering the scalp overlying the entire prefrontal cortex in the left and right hemispheres. The distances between the NIRS source and the detector (channel length) were set to 3.5 cm (diagonal) and 4.2 cm (vertical, horizontal), and the sampling rate was fixed at 1.8 Hz. In each optode, the DYNOT shot two wavelengths of light (760 nm

and 830 nm) through the scalp. Fourteen optodes (an optode plays two roles: emitter and detector) were pushed onto the forehead using the headgear specially designed for the experiment such that they were in contact with the scalp. The headgear was comfortably attached to the subject's head using a soft elastic band.

2.5. Data Preprocessing. The fNIRS-measured light intensities acquired from the DYNOT were converted to the hemoglobin concentration changes, ΔHbO , and ΔHbR , using the MATLAB® toolbox NIRS-SPM (The MathWorks Inc., Natick, MA, USA). The toolbox utilizes the modified Beer-Lambert law [48] to calculate the ΔHbO and ΔHbR from optical density changes using the differential path length factor for each wavelength and extinction coefficients for HbO and HbR. The time series of ΔHbO and ΔHbR from all channels were low-pass filtered at a frequency of 0.1 Hz to remove cardiac signal, respiration, and Mayer wave systemic oscillations [35]. A fourth-order Butterworth low-pass filter was used [67], and the filtered data were then used to calculate the channel-wise mean across all subjects to determine the overall effects of HD-tDCS. ΔHbR signals did not show noticeable changes, when compared with ΔHbO over the 10 min stimulation period; therefore, we focused solely on ΔHbO . Because the fNIRS data is susceptible to baseline drifts, the signal was corrected by subtracting a curve of fourth-order polynomial that fitted the measured baseline signal [56].

2.6. Resting-State Functional Connectivity. The functional connectivity analysis was conducted for every phase of the experiment. The analysis at each phase was further divided into the following three levels: the functional connectivity between all right hemisphere channels (intra-hemispheric connectivity), functional connectivity between all left hemisphere channels (intra-hemispheric connectivity), and functional connectivity of all the right vs. left hemisphere channels (inter-hemispheric connectivity). The connectivity strength of the neuronal populations underlying the prefrontal cortex was expressed in terms of the temporal correlation [68] of the regional hemodynamics by calculating Pearson's correlation coefficient. Pearson's correlation coefficients were calculated at all three levels during all the stages of the experiment to produce functional connectivity matrices between the desired set of channels. The rows and columns of these matrices represent the channel numbers, while the elements of the matrices were the correlation coefficients of the matching channels. For the right hemisphere intraconnectivity matrix, we calculated the Pearson correlation coefficients between the time series data (ΔHbO) of every possible pair of the first 16 channels (channels 1–16). Similarly, the left hemisphere intraconnectivity matrix was calculated from the next 16 channels (channels 17–32). The inter-hemispheric connectivity matrix was determined by calculating the Pearson correlation coefficients between the time series data (ΔHbO) of each channel in the right hemisphere (channels 1–16) with all of the channels in the left hemisphere.

After the correlation matrices were calculated, a graph theory [69, 70] analysis was conducted to evaluate the

functional connectivity. In this analysis, the channels were considered nodes of the network and the connections between the channels were considered the edges of the network. Weak and insignificant links may represent spurious connections, especially in the functional and effective networks that tend to obscure the topology of strong and significant connections and are therefore often discarded by applying an absolute or a proportional weight threshold [71]. Therefore, we set the threshold value and then set the correlation coefficient values greater than the threshold value to "1" and those less than the threshold to "0" in order to binarize the connectivity matrices, similar to image thresholding in image processing [72]. Therefore, only the coefficients of the channels with significant connection strengths were retained as authentic connections. To avoid a random selection of the threshold value, all networks were characterized across a range of 0.5 to 0.9, with an increment of 0.1, and the graph theory parameters were analyzed as a function of the threshold. A starting threshold value of 0.5 was selected because it defines the connection strength among the channels, in order to ensure that the Pearson correlation coefficients are statistically significant. According to the matrix representation of the graphs, each matrix exactly defines a binary and undirected graph [73, 74]. For analyzing the network, we computed the most commonly used metrics: connection density, global and nodal degree, nodal efficiency, global clustering coefficient, and network global efficiency [75]. The network connection density and global degree describe the wiring cost of the entire network. The nodal degree defines the number of connections that the brain area under each channel makes with the rest of the brain areas of interest. Nodal degree is important for computing the effects of individual channels. This metric can be helpful for finding the channel with the greatest increase in connectivity relative to the applied stimulation. The nodal network efficiency indicates the value of a node for efficient communication through the network. This metric shows the channel with the maximum efficiency enhancement resulting from stimulation. The network clustering coefficient indicates the connectivity between the neighbors of each node. The global network efficiency indicates the quality of effective communication in the network because it is primarily influenced by short paths in the brain network.

The computation for graph theoretic metrics was performed by using MATLAB® toolbox FC-NIRS [75] and our own MATLAB® code. The statistical analysis of the measured fNIRS data, including computation of Pearson's correlation coefficients, was also executed by using MATLAB®. The Wilcoxon-Mann-Whitney (or rank-sum) test was utilized to confirm that differences between experimental phases were significant. The significance of the data was tested with a confidence level of $p < 0.05$.

3. Results

First, the effects of HD-tDCS on ΔHbO were examined in the pre-, intra-, and poststimulation phases. Figure 2 shows the time series ΔHbO means calculated from the averaged data of individual subjects for the activated channels. The ΔHbO

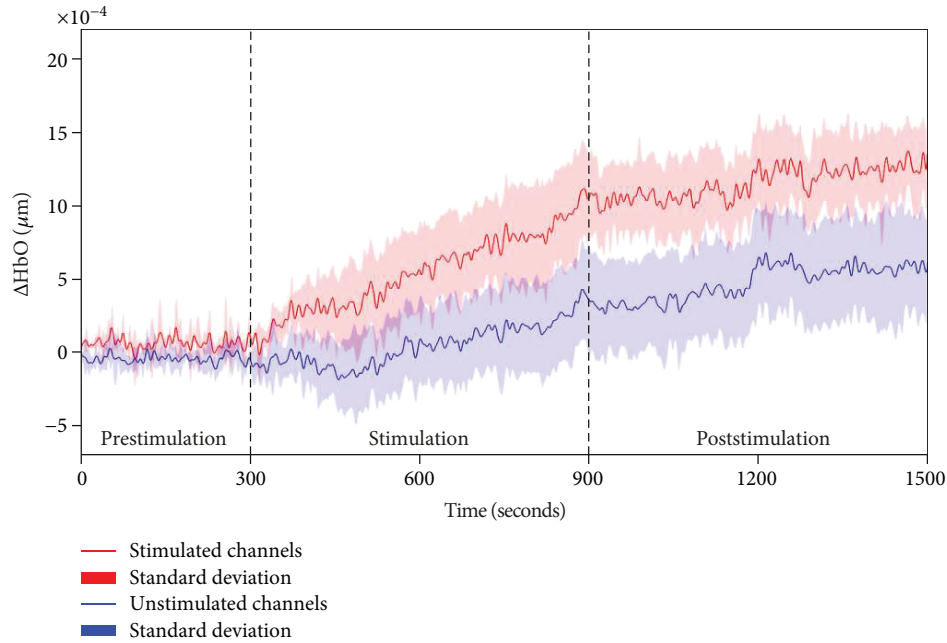


FIGURE 2: Comparison between stimulated channels (those underneath HD-tDCS) and unstimulated channels (ΔHbO values were averaged over all subjects).

values increased significantly after the start of the stimulation phase at 300 s (Wilcoxon rank-sum test, $p < 0.05$). The response continued to increase after the initial rise and continued through the stimulation phase. After the stimulation phase ended, the ΔHbO stabilized at the maximum level, where it remained throughout the entire poststimulation phase.

Figure 3 shows the correlation matrices for all phases of the experiment. Connectivity was present in the initial prestimulation phase and was focused in the center of the matrix. During the stimulation phase, the connectivity pattern from the initial phase was altered, but it was intensified and distributed, which indicated an increase in connectivity across the prefrontal region. After stimulation, the poststimulation phase showed a significant increase throughout the entire prefrontal cortex. The thresholded matrices (by 0.8) clearly showed a significant difference between pre- and poststimulation phases. The functional connectivity before stimulation in Figure 3(b) was 11% areawise, during stimulation was 30%, and after stimulation was 54%.

The correlation matrices (i.e., Figure 3(b)) were further analyzed by splitting it into smaller matrices for different regions. Figures 4(a) and 4(b) show the intrahemispheric correlation maps for right and left hemispheres, respectively, during pre- and postphases of the experiment.

The connectivity increased in both hemispheres; interestingly, the right hemisphere (the stimulated hemisphere) showed a greater increase in connectivity than did the left hemisphere. Figure 4(a) shows that the poststimulation connectivity in the right hemisphere was increased by 4.5 times (prestimulation, 12%; poststimulation, 55%) compared to the prestimulation connectivity, while that in the left hemisphere was increased by 2.5 times (prestimulation, 23%; poststimulation, 61%). Figure 4(c) shows the interhemispheric connectivity observed during the two stages. The connectivity

increased from a negligible level in the prestimulation phase to a significant level in the poststimulation phase. The interhemispheric connectivity increased 12.5 times (prestimulation, 4%; poststimulation, 51%). The increase in connectivity between the channels under the area of stimulation in the right hemisphere with the corresponding channels in the left hemisphere (prestimulation, 0%; poststimulation, 48%) was larger than those between the unstimulated channels of both hemispheres (prestimulation, 22%; poststimulation, 47%). The right hemispheric connectivity between the channels under the stimulation area and the unstimulated channels also showed a significant increase (prestimulation, 6%; poststimulation, 50%), as shown in Figure 4(d). The most significant increase was observed from the stimulated channels in the right hemisphere and their corresponding channels in the left hemisphere (prestimulation, 0%; poststimulation, 60%).

Graph theory metrics were calculated for ΔHbO at different threshold levels to determine the complete response as a function of threshold values. The results revealed similar trends for all threshold levels. Due to the similar trends, a threshold value of 0.8 was used when discussing the connectivity. Figures 5 and 6 show the network and nodal metrics that were calculated as a function of threshold values. The network connection density decreased with increasing threshold values. The differences between the prestimulation, stimulation, and poststimulation phases were clear in the metric of connection density. The differences between the phases remained nearly constant near the threshold value of 0.8 (Figure 5(a)). The global degree, mean of all nodal degrees, showed similar results as the connection density. The highest value of nodal degree in poststimulation was observed under the anode. In Figure 5(d), the global network efficiency decreased steadily with increasing threshold values in the poststimulation phase, whereas it remained nearly

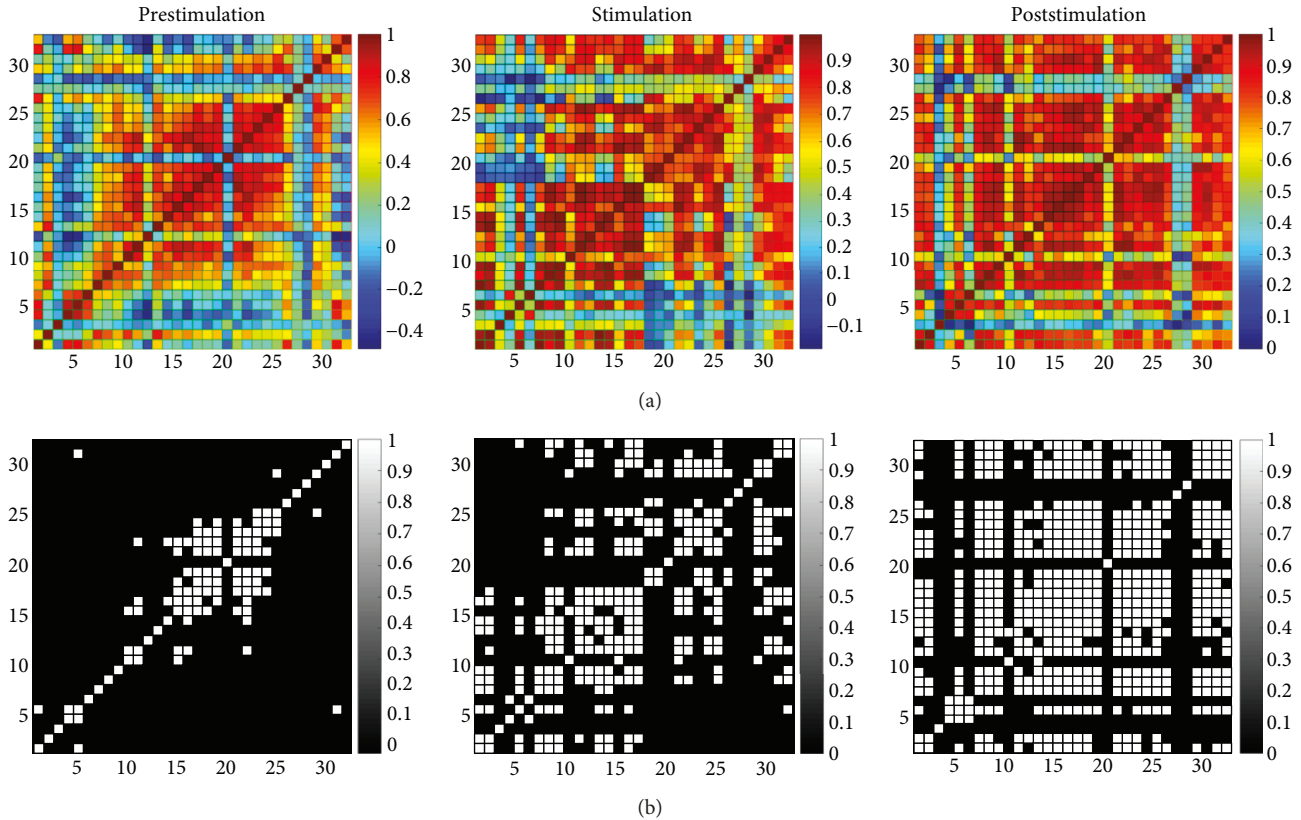


FIGURE 3: (a) Functional connectivity matrices for three stages and (b) binary matrices thresholded by Pearson's correlation coefficient 0.8.

constant in the prestimulation phase. There was a significant difference among the phases, and positive effects of the stimulation on the brain network were evident because the post-stimulation efficiency of the brain network was much higher than that of the prestimulation phase for all threshold levels. In terms of nodal network efficiency in Figure 6(b), channel 9 showed the highest efficiency in the poststimulation phase, which was also under the anode. The network clustering coefficient values were also reduced with increasing the threshold values. However, this metric was insensitive to the stimulation because a clear trend between the prestimulation and poststimulation phases was not found.

4. Discussion

To the best of our knowledge, this study is the first to evaluate the effects of HD-tDCS on the resting-state functional connectivity in the human prefrontal cortex using fNIRS and tDCS simultaneously. In each subject, we recorded 25 min of continuous fNIRS data before, during, and after stimulation on the right side of the prefrontal cortex and applied low-pass filtering to remove physiological noise. First, the correlation matrices of each phase were computed using the mean ΔHbO of all subjects. The poststimulation matrix exhibited a better connectivity than that observed in the prestimulation phase. Second, the interhemispheric and intrahemispheric matrices were separated to evaluate the overall effects of stimulation on different regions of interest. The connectivity enhancement rate was higher in the right

hemisphere than in the left hemisphere, because the right hemisphere was stimulated. We observed that stimulation increased the connectivity in all regions but at different levels. Finally, we used the functional connectivity matrices in each phase to calculate graph theory metrics. The results in Figure 5 showed that the connectivity improved across the phases. Figure 6 shows the channels and regions with a higher improvement. The resulting graph theory metrics clearly identified the prestimulation and poststimulation phases. These results suggest an important relationship between the effects of HD-tDCS and the resting-state prefrontal connectivity.

In almost all subjects, the ΔHbO increased at the time of stimulation. This supports the results in the early studies showing increased hemodynamic responses at the time of stimulation [49]. However, such trends differed among subjects. Some subjects showed a faster increase with stimulation that reached a maximum value and stayed at that level for the rest of the stimulation period, while some exhibited a slower increase that did not reach a plateau value. Interestingly, hemodynamic signals in most subjects did not return to baseline, except in two subjects, which was consistent with previous studies involving anodal stimulation [76]. Moreover, for those two subjects who exhibited reductions in signals, their hemodynamic responses did not reach the initial baseline level (returned to only 50% of the increment) within 10 min after the end of stimulation. The increased volumes of oxygen in the blood supply are important for patients with brain degeneration because oxygen helps to eliminate toxic substances [31]. The effects with respect to ΔHbR were neither

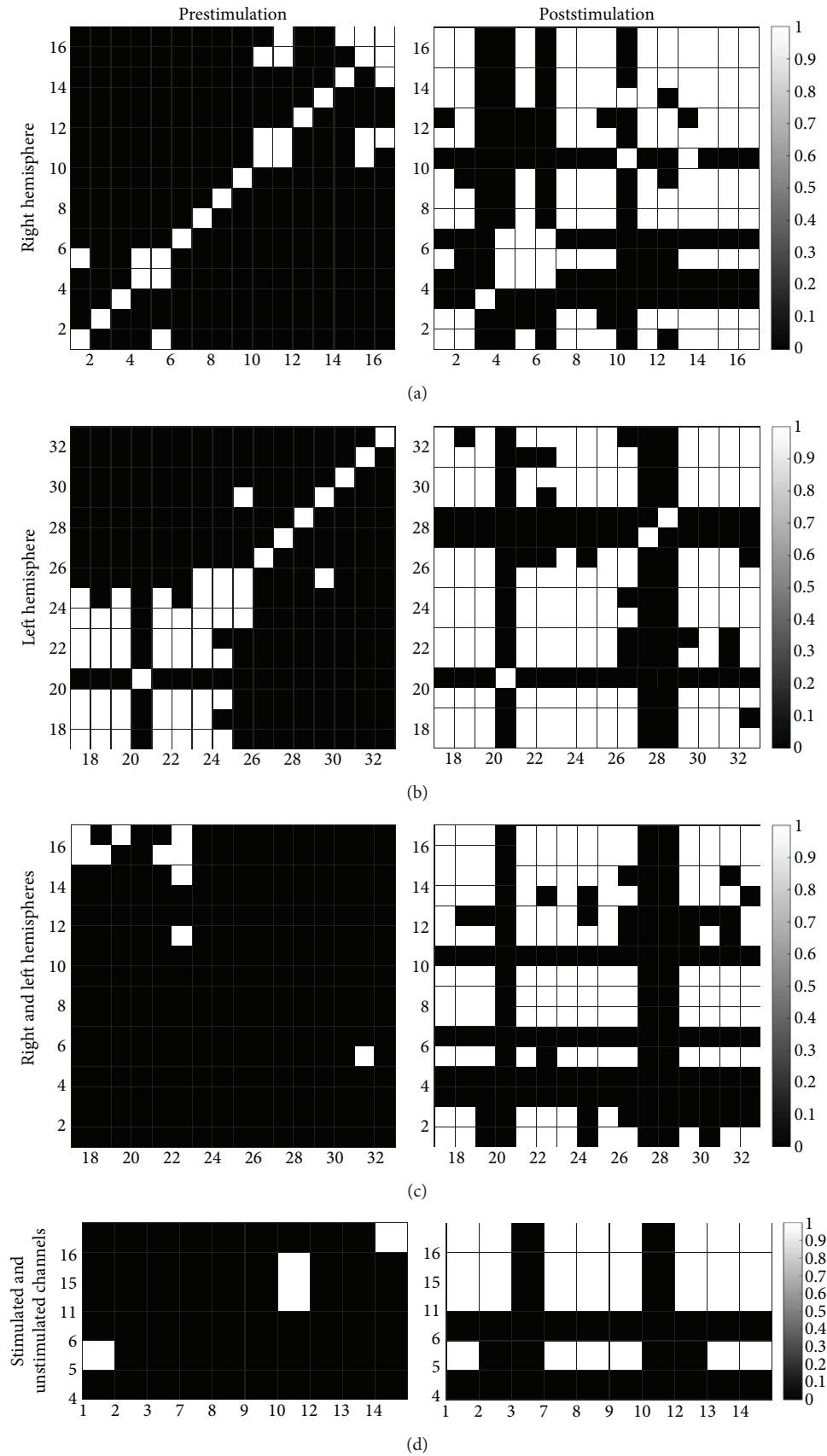


FIGURE 4: Connectivity binary matrices: (a) right intrahemispheric, (b) left intrahemispheric, (c) interhemispheric, and (d) between stimulated and unstimulated channels in the right prefrontal cortex.

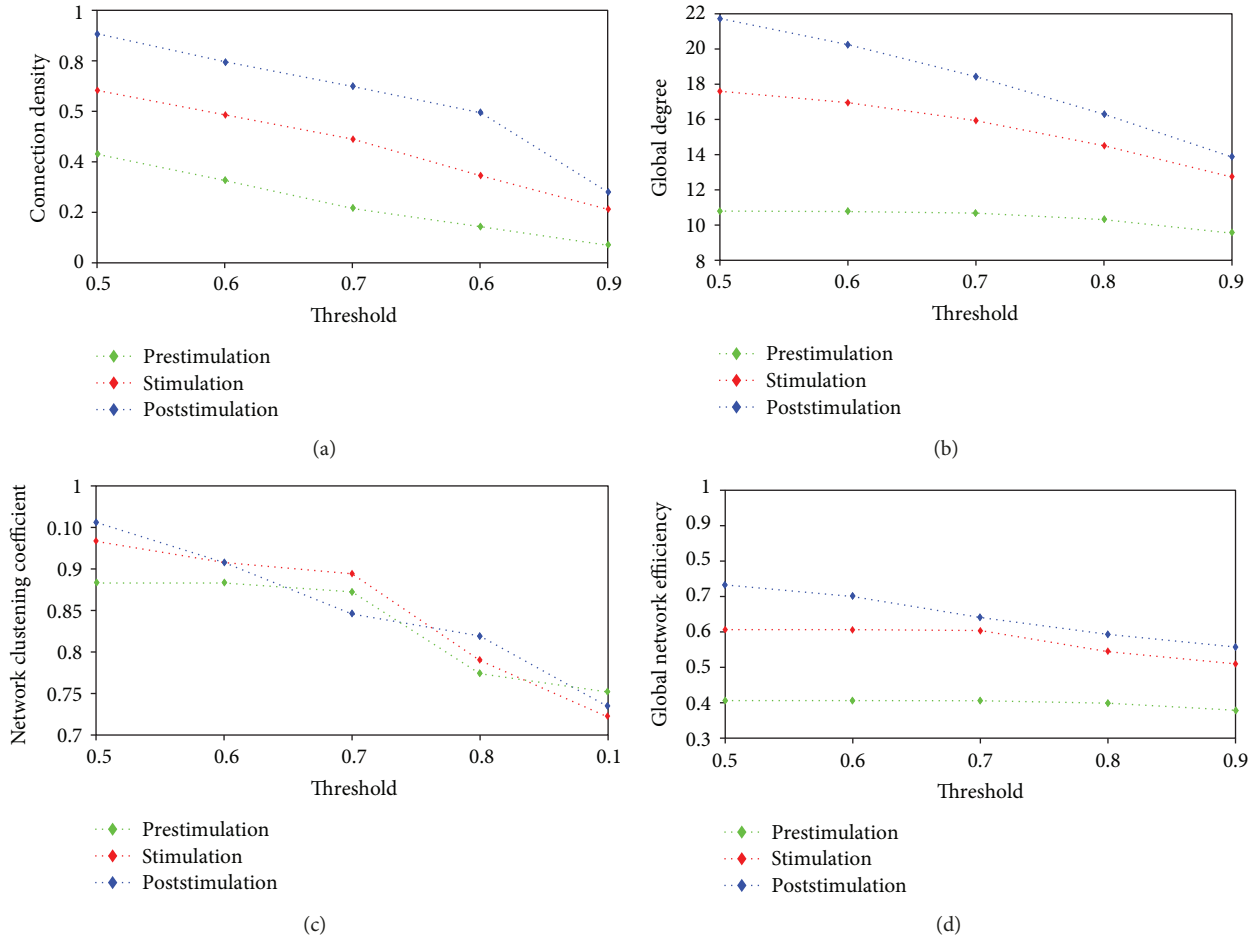


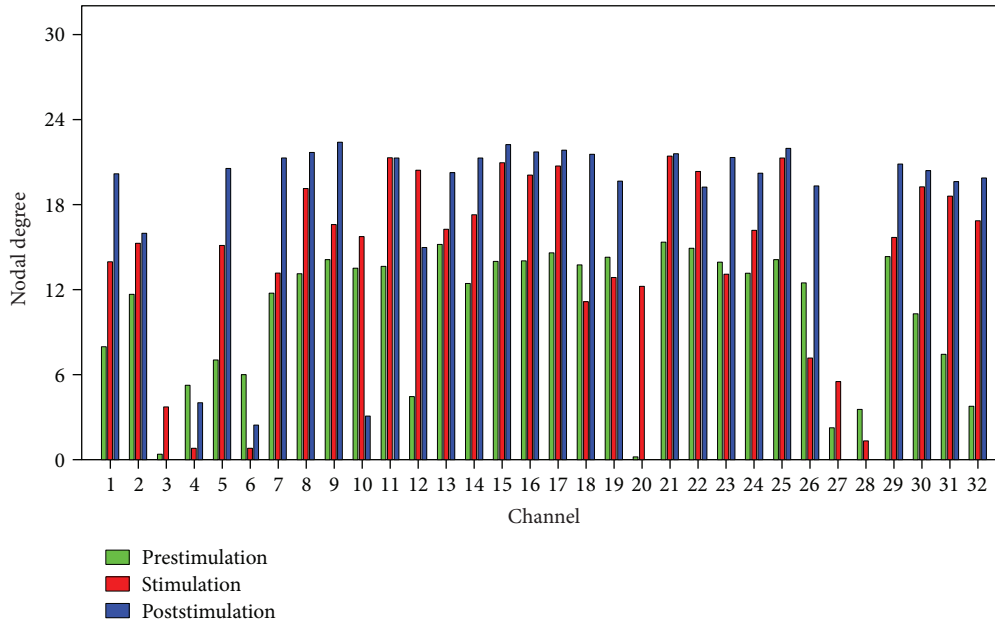
FIGURE 5: Global network metrics for all phases: (a) connection density, (b) degree, (c) clustering coefficient, and (d) network efficiency.

clear nor significant, in contrast with those observed in ΔHbO [35]. Because of this, the entire analysis was performed with ΔHbO alone.

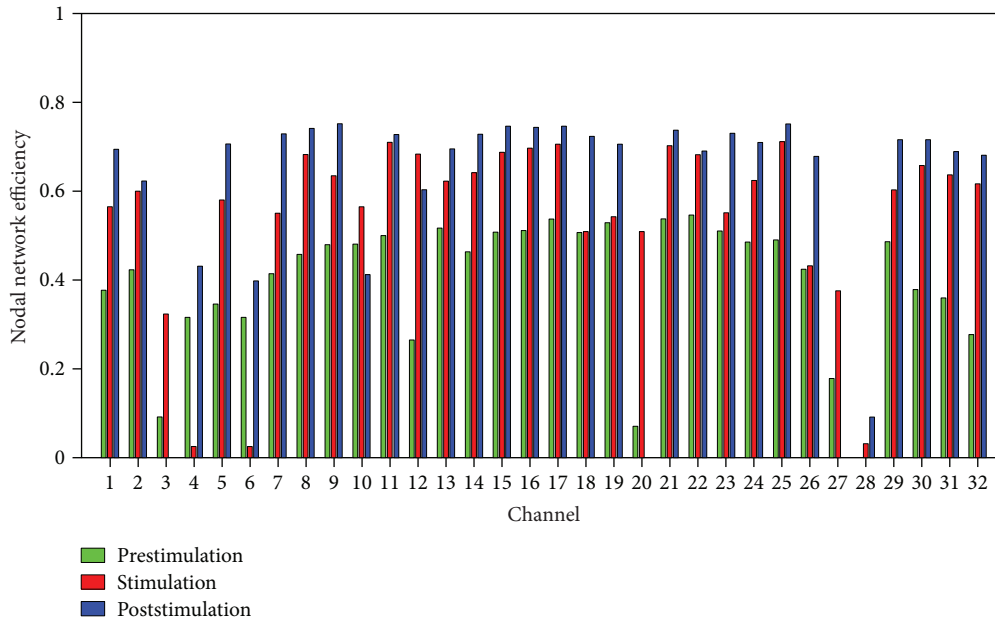
The brain area that performs working memory and several executive functions, including verbal and spatial reasoning, is the prefrontal cortex [77]. Accidental damage or degeneration of this area due to a brain disease, such as AD or frontotemporal dementia, causes various problems in daily life in our rapidly aging society. Several studies have used functional connectivity as a marker for detecting reduced cognitive performance, as it is directly related to cognitive performance [14, 78–82]. Therefore, fNIRS imaging is an important tool for the early detection of brain diseases, and combining it with tDCS is ideal due to the optical nature of fNIRS, which is not affected by the electric field during stimulation. AD, known as a disconnection disease, has been related to reduced connectivity in the human brain [83, 84]. Therefore, these connectivity analyses can help detect AD. Besides disease detection, the findings of this study provide evidence for the improvement in functional connectivity resulting from HD-tDCS, which supports the results of previous studies that have used different imaging modalities [28, 29]. The ability to focus and limit the effects of HD-tDCS to a stimulated area, which was observed in a previous study [35], is the reason for the greater enhancement in the

connectivity of the area underlying the stimulation montage. The stimulated hemisphere showed better overall connectivity improvement and, specifically, better interhemispheric connectivity of fNIRS channels under HD-tDCS stimulation. This approach can be used to rehabilitate the executive cognitive function impairments in patients with brain degeneration. Further studies should be conducted to determine the better stimulation pattern [85], the critical duration of stimulation, and the optimum amount of charge flow for specific patients. For instance, some early-stage patients might require a lower amount of charge, while others may require longer stimulation or even higher current intensity than in conventional experiments [86].

The network parameters used in this study were chosen to reflect the basic aspects of functional network organization [71, 87]. We computed the node degree to identify the amount of connectivity of each node, the connection density to investigate the overall wiring cost of the network, the clustering coefficient to monitor the ability to form local networks, the nodal efficiency to examine the importance of each channel in effective communication, and global efficiency to show the integration of the network in order to evaluate the overall effectiveness of rapid information transfer between nodes in the network. These parameters are used primarily to describe functional connectivities in the human



(a)



(b)

FIGURE 6: Nodal network metrics for all phases: (a) degree and (b) network efficiency.

brain. The limitation of the size of the network did not allow for a deeper brain network analysis by including the parameters like, but not limited to, nodal betweenness or modularity. We analyzed the results and found that HD-tDCS increased the overall interregional connections in the brain. These new connections will eventually shorten the connection paths to enhance the efficiency of the underlying brain network. The functional connectivity assessments based on these graph theory metrics, although relatively new in the field of neuroscience, have shown promising results for various applications, including different brain degenerative diseases [88–91].

The spatial resolution of fNIRS was a limitation of the current study. A detailed network analysis involving more network metrics at different depths in the brain regions could have been achieved by utilizing the 3D imaging approach of fNIRS [56], which has a better spatial resolution. We did not employ the 3D approach at this stage because we wanted to cover the whole prefrontal region with 32 channels, which would require a larger number of optodes than what was currently available. In the future, studies using the bundled optode approach can be conducted to determine the effects of stimulation at different depths in the cortex. Another limitation to the current study was the absence of short

separation channels that could help to remove skin-related artifacts, especially with respect to the application of tDCS, such as skin erythema resulting from vasodilation [92]. The signal from a short separation channel can illustrate the response from the skin, which can be subtracted from the fNIRS signal to enable the exclusion of skin artifacts. Thus, future studies should incorporate the short separation channel.

5. Conclusions

In this paper, the effect of HD-tDCS on the resting-state functional connectivity in the prefrontal cortex was demonstrated using functional near-infrared spectroscopy. The results revealed that ΔHbO was increased by the stimulation and the increased levels were maintained even after the stimulation was finished. By systematically analyzing the interhemispheric, intrahemispheric, and interregional connectivities, the results indicated that stimulation increased the connectivity in all areas, but the effects were greater in the area of stimulation than in the other areas. The overall functional connectivity of the stimulated hemisphere, as well as the interhemispheric connectivity of the stimulated area with the corresponding area of the other hemisphere, was large. Finally, the graph theory metrics showed significant differences between the phases of the experiment, which strengthened our results and indicated that functional connectivity was improved in this study. Our findings can be further enhanced and utilized in clinical procedures to treat executive cognitive function impairments in patients with degenerative brain diseases.

Data Availability

The fNIRS data used to support the findings of this study are available from the corresponding author upon request.

Conflicts of Interest

The authors declare that they have no conflicts of interest. This research was conducted in the absence of any commercial or financial relationship that could be construed as a potential conflict of interest.

Acknowledgments

This work was supported in part by the National Research Foundation (NRF) of Korea under the auspices of the Ministry of Science and ICT, Republic of Korea (grant no. NRF-2017R1A2A1A17069430) and by the Open Laboratory Operational Business Developing and Diffusing the Regional Specialization Technology funded by the Busan Institute of S&T Evaluation and Planning (BISTEP).

References

- [1] M. C. De LaCoste and C. L. White, "The role of cortical connectivity in Alzheimer's disease pathogenesis: a review and model system," *Neurobiology of Aging*, vol. 14, no. 1, pp. 1–16, 1993.
- [2] R. J. Perry and J. R. Hodges, "Attention and executive deficits in Alzheimer's disease: a critical review," *Brain*, vol. 122, no. 3, pp. 383–404, 1999.
- [3] X. Delbeuck, M. Van der Linden, and F. Collette, "Alzheimer's disease as a disconnection syndrome?," *Neuropsychology Review*, vol. 13, no. 2, pp. 79–92, 2003.
- [4] K. T. Jones, F. Gözenman, and M. E. Berryhill, "The strategy and motivational influences on the beneficial effect of neurostimulation: a tDCS and fNIRS study," *NeuroImage*, vol. 105, pp. 238–247, 2015.
- [5] J. M. Chein and A. B. Morrison, "Expanding the mind's workspace: training and transfer effects with a complex working memory span task," *Psychonomic Bulletin & Review*, vol. 17, no. 2, pp. 193–199, 2010.
- [6] Y. Moriguchi and K. Hiraki, "Prefrontal cortex and executive function in young children: a review of NIRS studies," *Frontiers in Human Neuroscience*, vol. 7, p. 867, 2013.
- [7] A. C. Ehlis, S. Schneider, T. Dresler, and A. J. Fallgatter, "Application of functional near-infrared spectroscopy in psychiatry," *NeuroImage*, vol. 85, pp. 478–488, 2014.
- [8] Y. Kubota, M. Toichi, M. Shimizu et al., "Prefrontal activation during verbal fluency tests in schizophrenia—a near-infrared spectroscopy (NIRS) study," *Schizophrenia Research*, vol. 77, no. 1, pp. 65–73, 2005.
- [9] M. J. Herrmann, A. C. Ehlis, and A. J. Fallgatter, "Bilaterally reduced frontal activation during a verbal fluency task in depressed patients as measured by near-infrared spectroscopy," *The Journal of Neuropsychiatry and Clinical Neurosciences*, vol. 16, no. 2, pp. 170–175, 2004.
- [10] X. Liu, G. Sun, X. Zhang et al., "Relationship between the prefrontal function and the severity of the emotional symptoms during a verbal fluency task in patients with major depressive disorder: a multi-channel NIRS study," *Progress in Neuro-Psychopharmacology and Biological Psychiatry*, vol. 54, pp. 114–121, 2014.
- [11] T. Matsubara, K. Matsuo, M. Nakashima et al., "Prefrontal activation in response to emotional words in patients with bipolar disorder and major depressive disorder," *NeuroImage*, vol. 85, pp. 489–497, 2014.
- [12] Y. Nishimura, K. Takahashi, T. Ohtani, R. Ikeda-Sugita, K. Kasai, and Y. Okazaki, "Dorsolateral prefrontal hemodynamic responses during a verbal fluency task in hypomanic bipolar disorder," *Bipolar Disorders*, vol. 17, no. 2, pp. 172–183, 2015.
- [13] S. Pu, K. Nakagome, T. Yamada et al., "The relationship between the prefrontal activation during a verbal fluency task and stress-coping style in major depressive disorder: a near-infrared spectroscopy study," *Journal of Psychiatric Research*, vol. 46, no. 11, pp. 1427–1434, 2012.
- [14] H. Zhu, J. Xu, J. Li et al., "Decreased functional connectivity and disrupted neural network in the prefrontal cortex of affective disorders: a resting-state fNIRS study," *Journal of Affective Disorders*, vol. 221, pp. 132–144, 2017.
- [15] T. Ohta ni, K. Matsuo, K. Kasai, T. Kato, and N. Kato, "Hemodynamic responses of eye movement desensitization and reprocessing in posttraumatic stress disorder," *Neuroscience Research*, vol. 65, no. 4, pp. 375–383, 2009.
- [16] M. A. Nitsche and W. Paulus, "Excitability changes induced in the human motor cortex by weak transcranial direct current stimulation," *The Journal of Physiology*, vol. 527, no. 3, pp. 633–639, 2000.

- [17] H. L. Filmer, P. E. Dux, and J. B. Mattingley, "Applications of transcranial direct current stimulation for understanding brain function," *Trends in Neurosciences*, vol. 37, no. 12, pp. 742–753, 2014.
- [18] U. Ghafoor, S. Kim, and K.-S. Hong, "Selectivity and longevity of peripheral-nerve and machine interfaces: a review," *Frontiers in Neurobotics*, vol. 11, p. 59, 2017.
- [19] Y. Wei, K. Gu, X. Cui, C. Hao, H. Wang, and Y. Chang, "Strategies for feet massage robot to position the pelma acupoints with model predictive and real-time optimization," *International Journal of Control, Automation and Systems*, vol. 14, no. 2, pp. 628–636, 2016.
- [20] K.-S. Hong, N. Aziz, and U. Ghafoor, "Motor-commands decoding using peripheral nerve signals: a review," *Journal of Neural Engineering*, vol. 15, no. 3, article 031004, 2018.
- [21] M. A. Nitsche, D. Liebetanz, N. Lang, A. Antal, F. Tergau, and W. Paulus, "Safety criteria for transcranial direct current stimulation (tDCS) in humans," *Clinical Neurophysiology*, vol. 114, no. 11, pp. 2220–2222, 2003.
- [22] H. W. Gomma and J. Thomas, "Neurogenic bladder dysfunction: a novel treatment using robust model predictive control supported by noise attenuation technique," *International Journal of Control, Automation and Systems*, vol. 15, no. 6, pp. 2669–2680, 2017.
- [23] M. C. Pellicciari, D. Brignani, and C. Miniussi, "Excitability modulation of the motor system induced by transcranial direct current stimulation: a multimodal approach," *NeuroImage*, vol. 83, pp. 569–580, 2013.
- [24] R. Polanía, M. A. Nitsche, and W. Paulus, "Modulating functional connectivity patterns and topological functional organization of the human brain with transcranial direct current stimulation," *Human Brain Mapping*, vol. 32, no. 8, pp. 1236–1249, 2011.
- [25] R. Polanía, W. Paulus, A. Antal, and M. A. Nitsche, "Introducing graph theory to track for neuroplastic alterations in the resting human brain: a transcranial direct current stimulation study," *NeuroImage*, vol. 54, no. 3, pp. 2287–2296, 2011.
- [26] C. J. Stagg, J. O'shea, Z. T. Kincses, M. Woolrich, P. M. Matthews, and H. Johansen-Berg, "Modulation of movement-associated cortical activation by transcranial direct current stimulation," *European Journal of Neuroscience*, vol. 30, no. 7, pp. 1412–1423, 2009.
- [27] C. J. Stagg and M. A. Nitsche, "Physiological basis of transcranial direct current stimulation," *The Neuroscientist*, vol. 17, no. 1, pp. 37–53, 2011.
- [28] D. Keiser, T. Meindl, J. Bor et al., "Prefrontal transcranial direct current stimulation changes connectivity of resting-state networks during fMRI," *Journal of Neuroscience*, vol. 31, no. 43, pp. 15284–15293, 2011.
- [29] M. Mancini, D. Brignani, S. Conforto, P. Mauri, C. Miniussi, and M. C. Pellicciari, "Assessing cortical synchronization during transcranial direct current stimulation: a graph-theoretical analysis," *NeuroImage*, vol. 140, pp. 57–65, 2016.
- [30] A. C. Ehlis, F. B. Haeussinger, A. Gastel, A. J. Fallgatter, and C. Plewnia, "Task-dependent and polarity-specific effects of prefrontal transcranial direct current stimulation on cortical activation during word fluency," *NeuroImage*, vol. 140, pp. 134–140, 2016.
- [31] A. C. Merzagora, G. Foffani, I. Panyavin et al., "Prefrontal hemodynamic changes produced by anodal direct current stimulation," *NeuroImage*, vol. 49, no. 3, pp. 2304–2310, 2010.
- [32] C. J. Stagg, R. L. Lin, M. Mezue et al., "Widespread modulation of cerebral perfusion induced during and after transcranial direct current stimulation applied to the left dorsolateral prefrontal cortex," *Journal of Neuroscience*, vol. 33, no. 28, pp. 11425–11431, 2013.
- [33] S. K. Kessler, P. Minhas, A. J. Woods, A. Rosen, C. Gorman, and M. Bikson, "Dosage considerations for transcranial direct current stimulation in children: a computational modeling study," *PLoS One*, vol. 8, no. 9, article e76112, 2013.
- [34] A. Datta, V. Bansal, J. Diaz, J. Patel, D. Reato, and M. Bikson, "Gyri-precise head model of transcranial direct current stimulation: improved spatial focality using a ring electrode versus conventional rectangular pad," *Brain Stimulation: Basic, Translational, and Clinical Research in Neuromodulation*, vol. 2, no. 4, pp. 201.e1–207.e1, 2009.
- [35] M. Muthalib, P. Besson, J. Rothwell, and S. Perrey, "Focal hemodynamic responses in the stimulated hemisphere during high-definition transcranial direct current stimulation," *Neuromodulation: Technology at the Neural Interface*, vol. 21, no. 4, pp. 348–354, 2017.
- [36] D. Edwards, M. Cortes, A. Datta, P. Minhas, E. M. Wassermann, and M. Bikson, "Physiological and modeling evidence for focal transcranial electrical brain stimulation in humans: a basis for high-definition tDCS," *NeuroImage*, vol. 74, pp. 266–275, 2013.
- [37] J. D. Richardson, P. Fillmore, A. Datta, D. Truong, M. Bikson, and J. Fridriksson, "Toward development of sham protocols for high-definition transcranial direct current stimulation (HD-tDCS)," *NeuroRegulation*, vol. 1, no. 1, pp. 62–72, 2014.
- [38] H. I. Kuo, M. Bikson, A. Datta et al., "Comparing cortical plasticity induced by conventional and high-definition 4 × 1 ring tDCS: a neurophysiological study," *Brain Stimulation: Basic, Translational, and Clinical Research in Neuromodulation*, vol. 6, no. 4, pp. 644–648, 2013.
- [39] C. S. Roy and C. S. Sherrington, "On the regulation of the blood-supply of the brain," *The Journal of Physiology*, vol. 11, no. 1-2, pp. 85–158, 1890.
- [40] D. Attwell and C. Iadecola, "The neural basis of functional brain imaging signals," *Trends in Neurosciences*, vol. 25, no. 12, pp. 621–625, 2002.
- [41] A. Antal, M. Bikson, A. Datta et al., "Imaging artifacts induced by electrical stimulation during conventional fMRI of the brain," *NeuroImage*, vol. 85, pp. 1040–1047, 2014.
- [42] Z. Turi, W. Paulus, and A. Antal, "Functional neuroimaging and transcranial electrical stimulation," *Clinical EEG and Neuroscience*, vol. 43, no. 3, pp. 200–208, 2012.
- [43] A. Cancelli, C. Cottone, F. Tecchio, D. Q. Truong, J. Dmochowski, and M. Bikson, "A simple method for EEG guided transcranial electrical stimulation without models," *Journal of Neural Engineering*, vol. 13, no. 3, article 036022, 2016.
- [44] A. Roy, B. Baxter, and B. He, "High-definition transcranial direct current stimulation induces both acute and persistent changes in broadband cortical synchronization: a simultaneous tDCS–EEG study," *IEEE Transactions on Biomedical Engineering*, vol. 61, no. 7, pp. 1967–1978, 2014.
- [45] B. Chance, Z. Zhuang, C. UnAh, C. Alter, and L. Lipton, "Cognition-activated low-frequency modulation of light absorption in human brain," *Proceedings of the National Academy of Sciences*, vol. 90, no. 8, pp. 3770–3774, 1993.

- [46] A. D. Edwards, C. Richardson, P. Van Der Zee et al., "Measurement of hemoglobin flow and blood flow by near-infrared spectroscopy," *Journal of Applied Physiology*, vol. 75, no. 4, pp. 1884–1889, 1993.
- [47] D. A. Boas, C. E. Elwell, M. Ferrari, and G. Taga, "Twenty years of functional near-infrared spectroscopy: introduction for the special issue," *NeuroImage*, vol. 85, no. 1, pp. 1–5, 2014.
- [48] M. Cope and D. T. Delpy, "System for long-term measurement of cerebral blood and tissue oxygenation on newborn infants by near infra-red transillumination," *Medical and Biological Engineering and Computing*, vol. 26, no. 3, pp. 289–294, 1988.
- [49] B. Khan, T. Hodics, N. Hervey, G. Kondraske, A. M. Stowe, and G. Alexandrakis, "Functional near-infrared spectroscopy maps cortical plasticity underlying altered motor performance induced by transcranial direct current stimulation," *Journal of Biomedical Optics*, vol. 18, no. 11, article 116003, 2013.
- [50] M. Muthalib, B. Kan, K. Nosaka, and S. Perrey, "Effects of transcranial direct current stimulation of the motor cortex on prefrontal cortex activation during a neuromuscular fatigue task: an fNIRS study," in *Oxygen Transport to Tissue XXXV*, S. Huffel, G. Naulaers, A. Caicedo, D. F. Bruley, and D. K. Harrison, Eds., vol. 789 of *Advances in Experimental Medicine and Biology*, pp. 73–79, Springer, New York, NY, USA, 2013.
- [51] M. R. Bhutta, K.-S. Hong, B. M. Kim, M.-J. Hong, Y. H. Kim, and S. H. Lee, "Note: three wavelengths near-infrared spectroscopy system for compensating the light absorbance by water," *Review of Scientific Instruments*, vol. 85, no. 2, article 026111, 2014.
- [52] S. Cutini, S. B. Moro, and S. Bisconti, "Functional near infrared optical imaging in cognitive neuroscience: an introductory review," *Journal of Near Infrared Spectroscopy*, vol. 20, no. 1, pp. 75–92, 2012.
- [53] A. Cristia, E. Dupoux, Y. Hakuno et al., "An online database of infant functional near infrared spectroscopy studies: a community-augmented systematic review," *PLoS One*, vol. 8, no. 3, article e58906, 2013.
- [54] J. Yang, S. Kanazawa, M. K. Yamaguchi, and I. Kuriki, "Cortical response to categorical color perception in infants investigated by near-infrared spectroscopy," *Proceedings of the National Academy of Sciences*, vol. 113, no. 9, pp. 2370–2375, 2016.
- [55] K.-S. Hong, M. R. Bhutta, X. Liu, and Y. I. Shin, "Classification of somatosensory cortex activities using fNIRS," *Behavioural Brain Research*, vol. 333, pp. 225–234, 2017.
- [56] H. D. Nguyen and K.-S. Hong, "Bundled-optode implementation for 3D imaging in functional near-infrared spectroscopy," *Biomedical Optics Express*, vol. 7, no. 9, pp. 3491–3507, 2016.
- [57] P. E. Grant, N. Roche-Labarbe, A. Surova et al., "Increased cerebral blood volume and oxygen consumption in neonatal brain injury," *Journal of Cerebral Blood Flow and Metabolism*, vol. 29, no. 10, pp. 1704–1713, 2009.
- [58] M. N. Kim, T. Durduran, S. Frangos et al., "Noninvasive measurement of cerebral blood flow and blood oxygenation using near-infrared and diffuse correlation spectroscopies in critically brain-injured adults," *Neurocritical Care*, vol. 12, no. 2, pp. 173–180, 2010.
- [59] K.-S. Hong and M. J. Khan, "Hybrid brain-computer interface techniques for improved classification accuracy and increased number of commands: a review," *Frontiers in Neuroinformatics*, vol. 11, p. 35, 2017.
- [60] A. Zafar and K.-S. Hong, "Detection and classification of three-class initial dips from prefrontal cortex," *Biomedical Optics Express*, vol. 8, no. 1, pp. 367–383, 2017.
- [61] A. R. Anwar, M. Muthalib, S. Perrey et al., "Effective connectivity of cortical sensorimotor networks during finger movement tasks: a simultaneous fNIRS, fMRI, EEG study," *Brain Topography*, vol. 29, no. 5, pp. 645–660, 2016.
- [62] X. S. Hu, K.-S. Hong, and S. S. Ge, "Reduction of trial-to-trial variability in functional near-infrared spectroscopy signals by accounting for resting-state functional connectivity," *Journal of Biomedical Optics*, vol. 18, no. 1, article 017003, 2013.
- [63] Z. Liu, M. Zhang, G. Xu et al., "Effective connectivity analysis of the brain network in drivers during actual driving using near-infrared spectroscopy," *Frontiers in Behavioral Neuroscience*, vol. 11, p. 211, 2017.
- [64] E. Kirilina, A. Jelzow, A. Heine et al., "The physiological origin of task-evoked systemic artefacts in functional near infrared spectroscopy," *NeuroImage*, vol. 61, no. 1, pp. 70–81, 2012.
- [65] K. Wang, M. Liang, L. Wang et al., "Altered functional connectivity in early Alzheimer's disease: a resting-state fMRI study," *Human Brain Mapping*, vol. 28, no. 10, pp. 967–978, 2007.
- [66] B. Christie, "Doctors revise declaration of Helsinki," *BMJ: British Medical Journal*, vol. 321, no. 7266, p. 913, 2000.
- [67] A. Zafar and K.-S. Hong, "Neuronal activation detection using vector phase analysis with dual threshold circles: a functional near-infrared spectroscopy study," *International Journal of Neural Systems*, vol. 28, article 1850031, 2018.
- [68] D. S. Shim, J. S. Jeon, and K. T. Kim, "New unambiguous delay-and-multiply acquisition schemes for Galileo E1 OS signals and its performance analysis," *International Journal of Control, Automation and Systems*, vol. 15, no. 6, pp. 2848–2858, 2017.
- [69] M. Allen-Prince, C. Thomas, and S. Yi, "Analysis of the effects of communication delays for consensus of networked multi-agent systems," *International Journal of Control, Automation and Systems*, vol. 15, no. 5, pp. 2320–2328, 2017.
- [70] X. Gong, Y. J. Pan, and A. Pawar, "A novel leader following consensus approach for multi-agent systems with data loss," *International Journal of Control, Automation and Systems*, vol. 15, no. 2, pp. 763–775, 2017.
- [71] M. Rubinov and O. Sporns, "Complex network measures of brain connectivity: uses and interpretations," *NeuroImage*, vol. 52, no. 3, pp. 1059–1069, 2010.
- [72] H. Abidi, M. Chtourou, K. Kaaniche, and H. Mekki, "Visual servoing based on efficient histogram information," *International Journal of Control, Automation and Systems*, vol. 15, no. 4, pp. 1746–1753, 2017.
- [73] F. S. Racz, P. Mukli, Z. Nagy, and A. Eke, "Increased prefrontal cortex connectivity during cognitive challenge assessed by fNIRS imaging," *Biomedical Optics Express*, vol. 8, no. 8, pp. 3842–3855, 2017.
- [74] K. U. Lee, J. Y. Lee, Y. H. Choi, and J. B. Park, "On stability and inverse optimality for a class of multi-agent linear consensus protocols," *International Journal of Control, Automation and Systems*, vol. 16, no. 3, pp. 1194–1206, 2018.
- [75] J. Xu, X. Liu, J. Zhang et al., "FC-NIRS: a functional connectivity analysis tool for near-infrared spectroscopy data," *BioMed Research International*, vol. 2015, Article ID 248724, 11 pages, 2015.
- [76] M. A. Nitsche, L. G. Cohen, E. M. Wassermann et al., "Transcranial direct current stimulation: state of the art 2008," *Brain*

- Stimulation: Basic, Translational, and Clinical Research in Neuromodulation*, vol. 1, no. 3, pp. 206–223, 2008.
- [77] A. K. Barbey, M. Koenigs, and J. Grafman, “Dorsolateral prefrontal contributions to human working memory,” *Cortex*, vol. 49, no. 5, pp. 1195–1205, 2013.
- [78] X. Li, Z. Jing, B. Hu et al., “A resting-state brain functional network study in MDD based on minimum spanning tree analysis and the hierarchical clustering,” *Complexity*, vol. 2017, Article ID 9514369, 11 pages, 2017.
- [79] J. Liu, M. Li, Y. Pan et al., “Complex brain network analysis and its applications to brain disorders: a survey,” *Complexity*, vol. 2017, Article ID 8362741, 27 pages, 2017.
- [80] A. Lombardi, S. Tangaro, R. Bellotti et al., “A novel synchronization-based approach for functional connectivity analysis,” *Complexity*, vol. 2017, Article ID 7190758, 12 pages, 2017.
- [81] T. Wu, D. Chen, Q. Chen et al., “Automatic lateralization of temporal lobe epilepsy based on MEG network features using support vector machines,” *Complexity*, vol. 2018, Article ID 4325096, 10 pages, 2018.
- [82] L. L. Zeng, H. Shen, L. Liu et al., “Identifying major depression using whole-brain functional connectivity: a multivariate pattern analysis,” *Brain*, vol. 135, no. 5, pp. 1498–1507, 2012.
- [83] A. Hafkemeijer, C. Möller, E. G. Dopper et al., “Resting state functional connectivity differences between behavioral variant frontotemporal dementia and Alzheimer’s disease,” *Frontiers in Human Neuroscience*, vol. 9, p. 474, 2015.
- [84] J. Wang, Q. Dong, and H. Niu, “The minimum resting-state fNIRS imaging duration for accurate and stable mapping of brain connectivity network in children,” *Scientific Reports*, vol. 7, no. 1, p. 6461, 2017.
- [85] L. E. Mancuso, I. P. Ilieva, R. H. Hamilton, and M. J. Farah, “Does transcranial direct current stimulation improve healthy working memory?: a meta-analytic review,” *Journal of Cognitive Neuroscience*, vol. 28, no. 8, pp. 1063–1089, 2016.
- [86] M. Vöröslakos, Y. Takeuchi, K. Brinyiczki et al., “Direct effects of transcranial electric stimulation on brain circuits in rats and humans,” *Nature Communications*, vol. 9, no. 1, p. 483, 2018.
- [87] D. J. Watts and S. H. Strogatz, “Collective dynamics of ‘small-world’ networks,” *Nature*, vol. 393, no. 6684, pp. 440–442, 1998.
- [88] F. Agosta, S. Sala, P. Valsasina et al., “Brain network connectivity assessed using graph theory in frontotemporal dementia,” *Neurology*, vol. 81, no. 2, pp. 134–143, 2013.
- [89] F. Skidmore, D. Korenkevych, Y. Liu, G. He, E. Bullmore, and P. M. Pardalos, “Connectivity brain networks based on wavelet correlation analysis in Parkinson fMRI data,” *Neuroscience Letters*, vol. 499, no. 1, pp. 47–51, 2011.
- [90] C. J. Stam, “Modern network science of neurological disorders,” *Nature Reviews Neuroscience*, vol. 15, no. 10, pp. 683–695, 2014.
- [91] B. M. Tijms, A. M. Wink, W. de Haan et al., “Alzheimer’s disease: connecting findings from graph theoretical studies of brain networks,” *Neurobiology of Aging*, vol. 34, no. 8, pp. 2023–2036, 2013.
- [92] S. Durand, B. Fromy, P. Bouyé, J. L. Saumet, and P. Abraham, “Vasodilatation in response to repeated anodal current application in the human skin relies on aspirin-sensitive mechanisms,” *The Journal of Physiology*, vol. 540, no. 1, pp. 261–269, 2002.

